# XVI. APPLIED PLASMA RESEARCH*

## A. Active Plasma Systems

### Academic and Research Staff

Prof. L. D. Smullin
Prof. R. J. Briggs
Prof. R. R. Parker
Prof. K. I. Thomassen

### Graduate Students

S. P. Hirshman
J. L. Kulp, Jr.
J. A. Mangano
M. I. Mirkin
G. H. Neilson
M. Simonutti
A. E. Throop
P. R. Widing

### RESEARCH OBJECTIVES

The research of the Active Plasma Systems Group is concerned with the dynamics of highly ionized plasmas and charged-particle beams, with particular emphasis on the understanding and exploitation of wave interactions in plasmas. Some of the major areas are listed below.

1. Cyclotron Resonance Plasma Source

The basic mechanisms of plasma generation and heating, using cylindrical electron-cyclotron resonance structures (Lisitano structures), are being studied; our ultimate goal is to improve the performance of this type of plasma source.

R. J. Briggs, R. R. Parker

2. Wave Studies at Lower Hybrid Frequency

The program of studying wave propagation near the lower hybrid frequency in a magnetized plasma continues, with emphasis on discovering the mechanisms by which plasma can absorb energy at frequencies near the lower hybrid resonance. Of present interest are dispersion and absorption by the linear processes of viscous damping and mode conversion, and also by the nonlinear process of parametric excitations.

R. J. Briggs, R. R. Parker

3. Direct Conversion

Techniques for direct conversion of plasma energy to electricity will be theoretically examined. A traveling-wave scheme has been investigated in detail, and variations of this method are being developed to improve conversion efficiency.

R. J. Briggs

4. Ion Heating in Plasmas

Plasma heating by RF absorption at the lower hybrid resonance is being investigated experimentally in a mirror-confined plasma. Ion and electron temperature

*This work is supported by the National Science Foundation (Grant GK-28282X).

measurements and coupling impedances are being determined.

K. I. Thomassen

5. Plasma Production and Heating by Electron Beams

We are producing a steady (dc), hydrogen plasma by "draining" the plasma from two opposed beam-plasma discharges at opposite ends of a drift region. The electron beams do not enter the drift region. Our goal is to achieve parameters $n > 10^{11}$, Te > 10-20 eV, $n\mp/n_o > 60\text{-}70\%$.

We are studying techniques for injecting powerful charged beams into a toroidal system (Alcator) for initial production and heating of the plasma.

L. D. Smullin, K. I. Thomassen, R. R. Parker

6. Microwave Scattering from Beam-Plasma Interactions

The technique of microwave scattering will continue to be used to diagnose instabilities generated by beam-plasma interactions. An external plasma source will be used so that the interaction can be studied over a wider range of beam power and perveance, with the same equilibrium plasma configuration. Of particular interest are measurement of the saturation amplitude of the instability and comparison of our results with existing theories.

R. R. Parker

## 1. OBSERVATION OF WAVE PROPAGATION IN A MAGNETIZED PLASMA NEAR THE LOWER HYBRID RESONANCE

### Introduction

In a previous report[1] we analyzed wave propagation in a magnetized plasma near the lower hybrid resonance, according to collisionless cold-plasma theory. The motivation for that work was its application to the design of the microwave lower hybrid plasma heating experiment for the M.I.T. Alcator, a high magnetic field Tokamak type of plasma device that is now under construction.

The model in our wave-propagation analysis is that of a plasma uniform in the z direction, uniformly magnetized in the z direction, and with the plasma density gradients in a direction transverse to z. The location of the source of excitation of the wave in the model is at the zero-density edge of the plasma. We examined excitation both localized and of infinite extent in the z direction, imposing a single wave number, $k_{||}$.

We predicted some effects that are interesting and very important to the design of the lower hybrid heating experiment. This report discusses results of a small-scale experiment set up to study these phenomena. This experiment allows us to use measurement techniques, which will not be possible in the Alcator experiment, such as the

insertion of RF probes into the main plasma region to study the nature of the wave. The plasma parameters of this small system are extremely modest, and the wave-excitation power extremely low, compared with those in the Alcator experiment. Under these conditions, the scaling of some parameters is still possible, but with low-power excitation there will not be significant heating, and therefore nonlinear effects will probably not be detected.

## Experiment

Figure XVI-1 is a schematic diagram of the plasma system for the wave experiment. The plasma was generated by ~20 W of 2.45 GHz microwave power fed into a helical spiral attached to the center conductor of the feeding transmission line. The spiral is fitted inside of a copper cylinder, of 1.25 in. radius, 4 in. long, attached to the outer conductor of the transmission line. The nearly uniform magnetic field is adjusted to near electron-cyclotron resonance. The background gas is hydrogen at a pressure of $\sim 2 \times 10^{-4}$ μm.

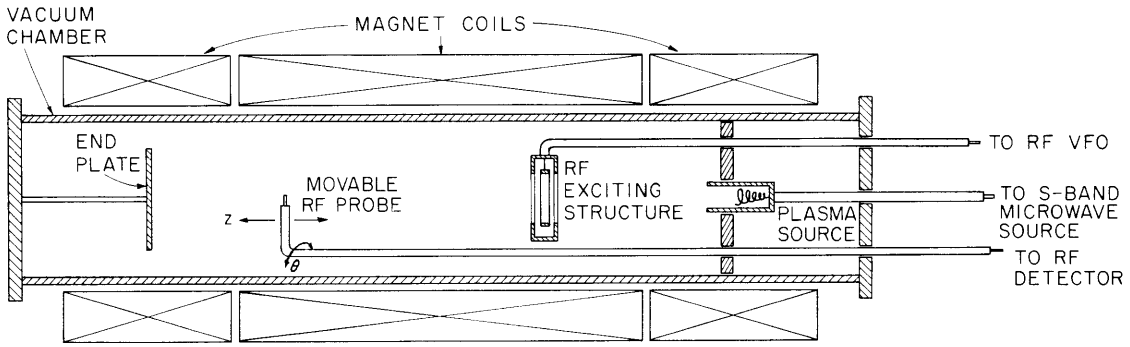


Fig. XVI-1. Plasma system for the wave experiment.

The plasma column produced by this scheme has a peak density on axis of $\sim 10^{10}/cm^3$. The density decreases slowly with increasing radius up to the 1.25 in. radius of the plasma-generating structure. At this radius, the density decreases sharply to a lower value and again decreases slowly with increasing radius.

The wave excitation is produced by an annular structure concentric with the plasma column consisting of a circular metal ring connected to the center conductor of the incoming transmission line. The ring is surrounded by a shell connected to the outer conductor. Spacing and insulation of the components is achieved by means of annular teflon inserts. The potential produced by this structure is a trapezoidal pulse in the z direction which under proper conditions may be satisfactorily treated in the analysis as an impulse. The RF input to this

structure is supplied by a variable-frequency oscillator.

The nature of the oscillation produced in the plasma is studied by observing the signal measured on a movable probe placed in the plasma. The probe is a dipole structure producing a balanced output signal that is fed into a differential amplifier and detected by means of a spectrum analyzer operated as a receiver. The probe can be moved independently in the axial and the azimuthal directions. The latter actually produces a radial scan across the plasma. Provided there is azimuthal symmetry in this experiment, a complete mapping of the wave amplitude throughout the plasma column can be obtained with this probe.

Results

Typical sets of data are presented in Fig. XVI-2. Each set is taken at a fixed frequency, each individual curve at a fixed axial position labeled with respect to distance from the exciting source. The probe angle axis is directly proportional to the radial position of the probe. The relative height of each curve, with respect to the zero level marked at the ends, is proportional to the electric field strength at that probe position.

As predicted in the previous report,[1] the disturbance propagates into the plasma at an angle to the magnetic field. With the parameters of the present experiment, the angle is approximately $\phi = \omega/\omega_p$. This holds well under the conditions $\omega_{pe}^2 \ll \omega_{ce}^2$, $\omega^2 \gg \omega_{LH}^2$. Here $\omega_{pe}$ is the electron plasma frequency, $\omega_{ce}$ the electron gyro frequency, and $\omega_{LH}$ the lower hybrid frequency (which is approximately the ion-plasma frequency under the conditions of this experiment).

The trajectory of the maximum of the signal as it travels through the plasma allowing moderate radial density gradients is

$$z = \int_{x_0}^{x} \frac{-k_x}{k_z}\, dx + z_o = \int_{x_0}^{x} \left(\frac{-K_{\parallel}}{K_{\perp}}\right)^{1/2} dx + z_o,$$

where $K_{\parallel}$ and $K_{\perp}$ are components of the plasma dielectric tensor. From this expression the relation $\phi = \omega/\omega_p$ may be obtained in the proper parameter regime.

At 100 MHz (Fig. XVI-2a), conditions are such that the disturbance propagates into the center of the plasma, although with considerable damping, within the 40-cm measurement region. The damping is still not completely understood and will not be fully discussed here. It is interesting to note that the two separate peaks merge at the center of the column, combine to form a disturbance of increased amplitude, and then separate again as they continue to propagate. In some data sets (not presented here) we found that the damping was not so great and the enhanced signal at the center of the column was actually larger in amplitude than that near the exciting source. This is a sort of

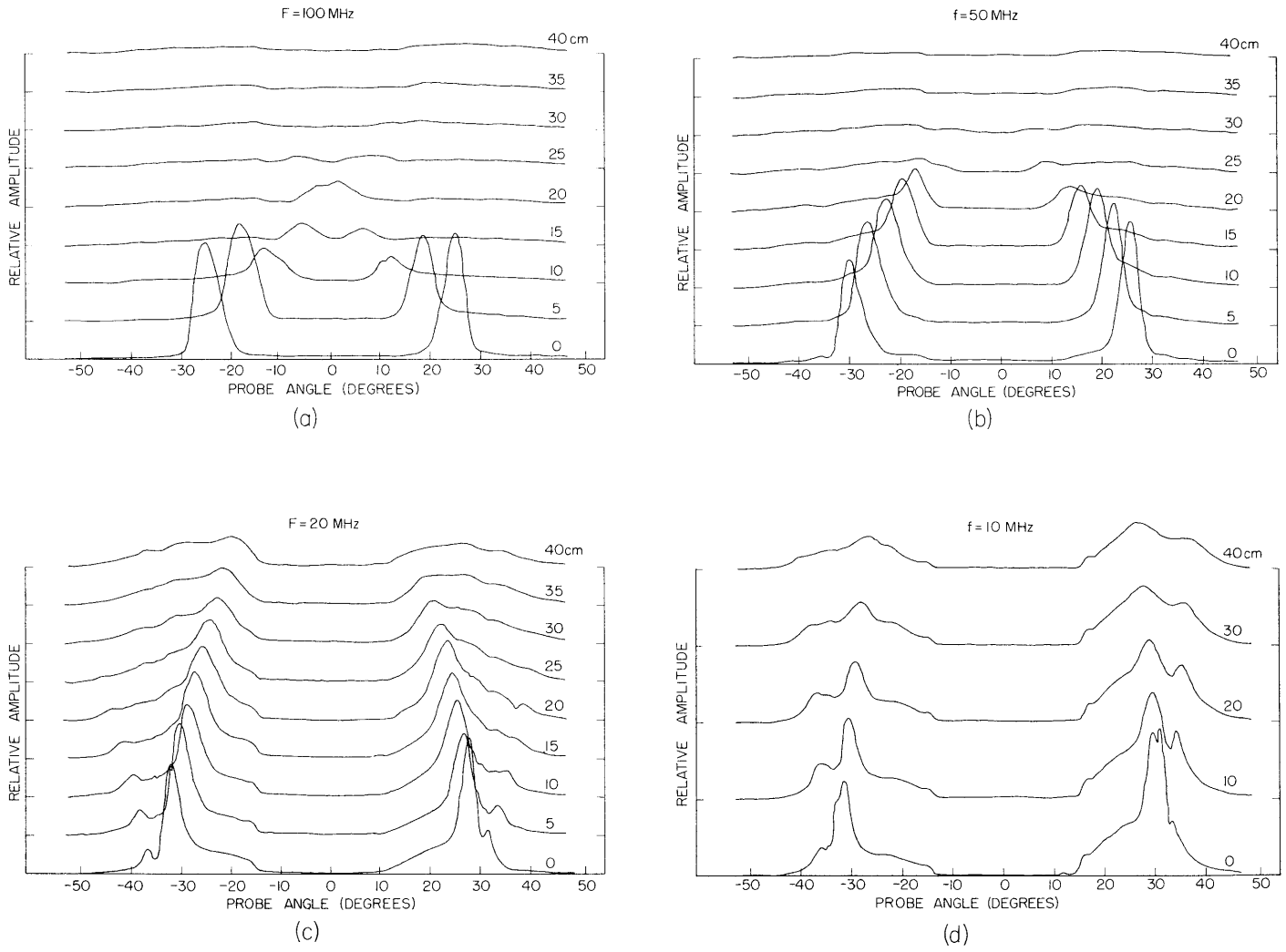


Fig. XVI-2. Results of the wave experiment.
(a) F = 100 MHz. (b) F = 50 MHz.
(c) F = 20 MHz. (d) F = 10 MHz.

focusing effect and could serve to produce strong fields at a central point in a plasma of proper symmetry.

The general appearance of the data here is similar to that presented by Fisher and Gould,[2] in the sense that the disturbance defines a sort of cone in the plasma. Important differences should be pointed out, however. Fisher and Gould present results at frequencies well above the lower hybrid frequency, while our data include measurements near lower hybrid resonance. Also, they use a point source located at the center of the plasma, while we use an annular source located at the outside edge of the plasma. This arrangement is of interest in a plasma heating scheme that requires power to be coupled to the plasma from a source removed from the main plasma region.

At 50 MHz (Fig. XVI-2b), we see that propagation is inward at approximately half the angle of the 100-MHz case, in agreement with the $\phi = \omega/\omega_p$ prediction. Again, the disturbance damps strongly as it reaches a certain radial position. This radial position corresponds to the region of large density gradient, and this gradient is believed to be responsible for the strong damping; however, the exact mechanism by which this takes place is not understood.

At 20 MHz (Fig. XVI-2c), the angle becomes shallow and we begin to see secondary disturbances traveling outward from the source. At these lower frequencies the shielding effect of the source is less effective in preventing outward propagation and the secondary disturbance appears.

At 10 MHz (Fig. XVI-2d), the hybrid resonance region of the plasma is near the outside edge of the column. Propagation (actually not an appropriate description, since the disturbance has no measurable phase shift, in accordance with theory) is nearly along the magnetic field, especially as the wave gets far into the plasma where the density increases to the hybrid resonance layer.

## Discussion

Unfortunately the strong damping at the radius of large density gradient masks effects of plasma density inhomogeneity on the wave. If the gradient were weaker, we would expect the angle of propagation to decrease as the density increases. The angle would become zero where the density corresponds to lower hybrid resonance.

We count on this effect in the Alcator experiment. The power should propagate inward at an angle of 90° near the edge of the plasma with the angle decreasing as the wave approaches the center of the plasma at the lower hybrid resonance region. Calculations show that the disturbance will travel a distance equivalent to several times around the torus before reaching the resonance region.

It is important that the heating experiment be done in a closed, toroidal system. In an open system the wave would reach the ends of the system, not yet having fully dissipated its wave energy into particle heating, and lose its remaining energy to the ends

of the machine. In a closed system the wave will become trapped inside the torus, and circulate. The wave amplitude will increase until the dissipation of power into heating, or possibly into nonlinear coupling to other waves, equals the power supplied by the source.

An important question to be raised is, Does the wave indeed follow the magnetic field lines as it approaches hybrid resonance so that the wave energy circulates around the torus? A preliminary measurement has been made to examine this question. A depression in the otherwise uniform magnetic field of the system was made by removing power from one of the magnet solenoid coils. This created a local mirror type of field of mirror ratio 1.35 and halfwidth of 20 cm. Under these conditions, the signal followed the curvature of the field lines. For this effect to take place in Alcator and in this experiment the magnetic field lines must be nearly coincident with constant density lines.

M. Simonutti, R. R. Parker, R. J. Briggs

References

1. R. R. Parker, Quarterly Progress Report No. 102, Research Laboratory of Electronics, M.I.T., July 15, 1971, pp. 97-111.
2. R. K. Fisher and R. Gould, Phys. Fluids 14, 857 (1971).

## 2. WARM-PLASMA EFFECTS ON RESONANCE CONE STRUCTURE

Previous work[1,2] has shown that excitation of a cold magnetized plasma by a localized source results in an RF electric field which is singular on the surface of a cone, having a half-angle equal to $(m/M)^{1/2} \sqrt{1 - \omega_{pi}^2/\omega^2}$ with respect to the magnetic field. This effect has also been amply demonstrated experimentally. Since the electrons may properly be treated as collisionless in the experimental configuration and also

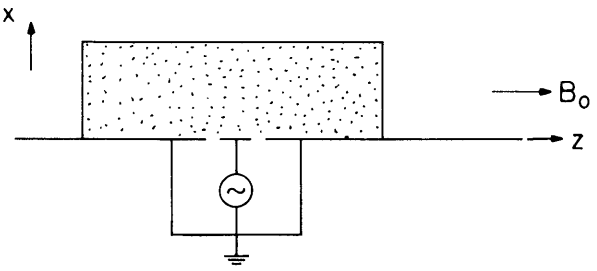


Fig. XVI-3. Slab geometry.

in the proposed experiment on Alcator, it is of interest to compute the effect of the streaming electrons on the structure of the resonance cone. This effect has been partially studied by Fisher and Gould[2] who neglected Landau damping. The purpose of this report is to assess the importance of Landau damping on their result.

Consider the simple slab geometry shown in Fig. XVI-3. We treat the plasma as homogeneous, bounded by a conducting wall at x = 0, in which a slot is cut to permit placement of an electrode connected to a voltage source. We model the potential at x = 0 as $\phi(x=0, z) = \delta(z)$ and Fourier-transform all variables in the z direction. Within the framework of electrostatics, the potential $\phi$ is determined for x > 0 by

$$\nabla \cdot \overline{\overline{K}} \cdot \nabla\phi = \frac{d}{dx} K_{\perp} \frac{d\phi}{dx} - \beta^2 K_{\parallel}\phi = 0. \tag{1}$$

Since wavelengths perpendicular to the field are assumed large compared with the Larmor radii, we take

$$K_{\perp} = 1 - \omega_{pi}^2/\omega^2$$

which is appropriate near lower hybrid frequency for $\omega_{pe}^2 \ll \omega_{ce}^2$, whereas

$$K_{\parallel} = -\frac{\omega_{pe}^2}{\beta^2 v_{th}^2} Z' \left(\frac{-\omega}{|\beta| v_{th}}\right).$$

Here $\beta$ is the Fourier-transform variable, Z is the plasma dispersion function, and other symbols have the usual meaning.

Solving (1) and applying the boundary condition, we get

$$\phi = \int_{-\infty}^{\infty} d\beta \exp\left[i\beta z + i|\beta| \sqrt{-\frac{K_{\parallel}}{K_{\perp}}}\, x\right]. \tag{2}$$

We first wish to obtain an asymptotic form for (2) in which we neglect Landau damping and use the asymptotic form for $-K_{\parallel}$,

$$-K_{\parallel} = \frac{\omega_{pe}^2}{\omega^2}\left(1 + \frac{3}{2}\frac{\beta^2 v_{th}^2}{\omega^2}\right). \tag{3}$$

The integration from $-\infty$ to 0 in (3) results in resonance occurring for z > 0, whereas the integration from 0 to $\infty$ yields resonance in the region z < 0. For simplicity, we

consider only the region $z > 0$, in which the potential can be written

$$\phi_+ = \int_0^\infty d\beta \exp\left[-i\beta z + i\beta \sqrt{-\frac{K_\parallel}{K_\perp}}\, x\right]. \tag{4}$$

By expanding $(-K_\parallel)^{1/2} \approx \omega_{pe}/\omega \left(1 + \frac{3}{4} \frac{\beta^2 v_{th}^2}{\omega^2}\right)$, we obtain, in normalized form,

$$\phi_+ = \frac{\epsilon}{z_o} F\left(\epsilon \frac{z - z_o}{z_o}\right), \tag{5}$$

where

$$\epsilon = \left(\frac{4}{9} \frac{z_o^2 \omega^2}{v_{th}^2}\right)^{1/3}$$

$$z_o = \frac{\omega_{pe}}{\omega \sqrt{1 - \omega_{pi}^2/\omega^2}}\, x$$

and

$$F(u) = \int_0^\infty dk \exp[-iku + ik^3/3]. \tag{6}$$

The function F(u) can be expressed in terms of Airy functions and their integrals, but this is not useful because (5) is correct only asymptotically, in which case (6) can be estimated directly by using the saddle-point technique. A saddle point exists at $k_s = \sqrt{u}$ for u positive; however, end-point contributions appear for u both positive and negative, and lead to the estimate

$$F(u) = \begin{cases} -\frac{i}{u} + \frac{\sqrt{\pi}}{u^{1/4}} \exp\left[-i\frac{2}{3}u^{3/2} - \frac{\pi}{4}\right] & u \to \infty \\ -\frac{i}{u} & u \to -\infty \end{cases} \tag{7}$$

The $1/u$ term represents the cold-plasma result for the resonance cones along the trajectory $z = z_o(x)$. The new result is the appearance of warm-plasma waves that are also excited by the structure. These should result in interference effects inside the

trajectory of the cone, and they have apparently been observed by Fisher and Gould.[2]

The question now arises, What effect will the Landau damping have on the interference structure predicted by (7)? In order that damping be negligible, it is necessary from (4), that

$$\mathrm{Im}\left(\beta_s \sqrt{-\frac{K_{\parallel}(\beta_s)}{K_{\perp}}}\, x\right) < 1, \tag{8}$$

where $\beta_s$ is the value of $\beta$ giving rise to the saddle point used in obtaining (7). Since $k_s = u^{1/2}$ and $k = \beta\left(\frac{9}{4}\frac{v_{th}^2}{\omega^2} z_o\right)^{1/3}$, we get

$$\beta_s = \frac{2}{3}\frac{\omega}{v_{th}}\left(\frac{z - z_o}{z_o}\right)^{1/2}.$$

Now if we insert this in (8) together with the expression for Im Z', we arrive at the condition

$$\sqrt{\pi}\,\frac{z_o\omega}{v_{th}}\left(\frac{9}{4}\frac{z_o}{z - z_o}\right)\exp\left(-\frac{9}{4}\frac{z_o}{z - z_o}\right) < 1. \tag{9}$$

Of course, (9) will be satisfied for z sufficiently close to $z_o$. The asymptotic form (7) is not valid there, however, since $u \to 0$ as $z \to z_o$. A useful way of applying the inequality (9) is to demand that n half-wavelengths of the oscillating part of the solution in (7) be undamped. The locus of z vs x along which the asymptotic phase is $n\pi$ is obtained by setting $\frac{2}{3}u^{3/2} = n\pi$. In unnormalized variables we get

$$z = z_o\left(1 + \left(\frac{9n\pi}{4}\right)^{2/3}\left(\frac{v_{th}}{z_o\omega}\right)^{2/3}\right).$$

Substituting in (9) results in an inequality determining $z_o$ or equivalently z, the axial position at which n half-wavelengths of oscillation should be visible. The calculation yields

$$z \gtrsim 30\, n\,\frac{v_{th}}{\omega}.$$

For the parameters of our experiment, this represents a sizable distance ~50 cm at 20 MHz for n = 1. This may explain why the interference effects have not been observed.

Finally, we note that this calculation seems to be verified by a numerical computation presented by Fisher and Gould. Their results show approximately 8 half-wavelengths at $z = 200\ v_{th}/\omega$, whereas our estimate predicts $z = 240\ v_{th}/\omega$ for 8 half-wavelengths to be visible.

R. R. Parker, R. J. Briggs

References

1. R. R. Parker, Quarterly Progress Report No. 102, Research Laboratory of Electronics, M.I.T., July 15, 1971, pp. 97-111.
2. R. K. Fisher and R. Gould, Phys. Fluids 14, 857 (1971).

## 3. PROPERTIES OF PLASMA COLUMNS CREATED BY CYLINDRICAL MICROWAVE STRUCTURES

A study of the properties of a plasma column created by a cylindrical microwave structure has been completed. The principal objective of this research was to make an accurate measurement of the radial density profile over a relatively wide density range. New techniques for rapid and accurate determination of density and temperature by the use of a very thin cylindrical probe were developed. The results will be presented in "Probe Measurements of Plasma Density in the Orbital-Motion-Limited Region," S. M. Thesis by John M. Tarrh III, Department of Electrical Engineering, M.I.T., in February, 1972.

R. R. Parker, R. J. Briggs

## 4. ENERGY RECOVERY FROM PLASMA STREAMS BY A DECELERATING WAVE

### Introduction

In this report, further results are presented on the theoretical analysis of a scheme[1] for energy recovery from energetic plasma streams by interaction with a decelerating electrostatic wave excited by a lumped-element transmission-line circuit. We first describe how particles are trapped when there is an adiabatic spatial variation of the wave amplitude and phase velocity, and we evaluate the trapping efficiency. Then we discuss the stability of trapped particles, and finally use our results to evaluate the overall recovery efficiency.

The one-dimensional, nonrelativistic equation of motion for a particle of mass m and charge q, acted on by a traveling electric field of magnitude $E_m(z)$, phase velocity v(z), and radian frequency $\omega$ can be normalized and written in the form[1]

$$\frac{d^2\phi}{d\tau^2} + \frac{dv_n}{dz}\left[1 + \frac{d\phi}{d\tau}\right]^2 - \gamma(z)\sin\phi = 0, \tag{1}$$

$$\frac{dz}{d\tau} = v_n(z)\left[1 + \frac{d\phi}{d\tau}\right], \tag{2}$$

where

$$\tau = \omega t, \qquad z = \frac{\omega z_a}{v(z=0)}, \qquad \text{with } z_a \text{ the physical dimension,}$$

$$v_n(z) = \frac{v(z)}{v(z=0)}$$

$$\gamma(z) = \frac{qE_m(z)}{m\omega v(z)} \tag{3}$$

$$\phi = \int_{z_i}^{z} \frac{\omega d\xi}{v(\xi)} - \omega t + \phi_i.$$

(Variables with i and f subscripts refer to initial and final values, respectively.) For the assumed adiabatic spatial variations of $E_m$ and v, the following linear approximations are justified over a limited range of z.

$$v_n(z) = v_{ni} - \alpha(z - z_i)$$

$$\gamma(z) = \gamma_i\left[1 + \frac{\alpha\lambda}{v_{ni}}(z - z_i)\right], \tag{4}$$

where

$$\alpha \equiv -\frac{1}{\omega}\frac{dv}{dz}\bigg|_{z=z_i} \ll 1$$

$$\lambda \equiv \frac{\gamma'/\gamma}{-v'/v}\bigg|_{z=z_i}$$

Physically, $\alpha$ represents the fractional change in phase velocity over a distance of $1/2\pi$ wavelengths, and $\lambda$ represents the ratio of the logarithmic gradient in $\gamma$ to the logarithmic gradient in the phase velocity.

Trapping Process

A nonlinear theory must be used to treat large-amplitude trapped-particle oscillations, untrapped particle transits through the potential troughs and crests, and the process whereby an untrapped particle becomes trapped by a decelerating wave. The key to this nonlinear theory is the development of an "energylike" expression obtained by multiplying Eq. 1 by $d\phi/d\tau$, which for the assumed adiabatic linear wave taper over a particle transit yields

$$\frac{d}{d\tau}(T+V_o) = P, \tag{5}$$

where

$$T = \frac{1}{2}\left(\frac{d\phi}{d\tau}\right)^2$$

$$V_o = \gamma_i \cos\phi$$

$$P = \alpha \frac{d\phi}{d\tau}\left[\left(1+\frac{d\phi}{d\tau}\right)^2 + \gamma_i\lambda(\tau+\phi-\phi_i)\sin\phi\right] + \mathcal{O}(\alpha^2).$$

Equation 2 has been used to eliminate z from Eq. 5. The "dissipation" function, P, is first-order in $\alpha$, a good expansion parameter, since adiabaticity requires $|\alpha| \ll 1$; $V_o$ is the zero-order potential function; T plays the role of a "kinetic-energy" term in the (noninertial) wave frame. To zero order in $\alpha$, Eq. 5 describes the familiar large-amplitude oscillations of a simple pendulum; the solution can be expressed in terms of elliptic integrals.

The change in total energy $(T+V_o)$ can be determined to first order in $\alpha$ by integrating the total "dissipation", P, along the zero-order particle trajectory. With this technique, we find the following expression for $\dot{\phi}_f^2 - \dot{\phi}_i^2$ for a particle with $(d\phi/d\tau)_i \equiv \dot{\phi}_i$ at $\phi_i = 0$ and $\dot{\phi}_f$ at $\phi_f = 2\pi$ (upper signs); the lower signs apply to motion in the opposite direction ($\dot{\phi}_i = 2\pi$, $\phi_f = 0$).

$$\frac{\dot{\phi}_f^2 - \dot{\phi}_i^2}{\alpha} = C_1(\gamma_i, \dot{\phi}_i) + \lambda C_2(\gamma_i, \dot{\phi}_i), \tag{6}$$

where

$$C_1 = 32\sqrt{\gamma_i}\,\frac{E(\chi)}{\chi} \pm 4\pi\left(1+\dot{\phi}_i^2+2\gamma_i\right)$$

$$C_2 = \frac{2\dot{\phi}_i^2}{\sqrt{\gamma_i}} \chi F(\chi) - 8\sqrt{\gamma_i}\,\frac{E(\chi)}{\chi} \mp 4\pi\gamma_i$$

$$\chi = \frac{1}{\left(1 + \frac{\dot{\phi}_i^2}{4\gamma_i}\right)^{1/2}}$$

$$E(\chi) = \int_0^{\pi/2} (1 - \chi^2 \sin^2\theta)^{1/2}\, d\theta$$

$$F(\chi) = \int_0^{\pi/2} \frac{d\theta}{(1 - \chi^2 \sin^2\theta)^{1/2}}.$$

With Eq. 6, we can map $\dot{\phi}^2$ from one wave crest to the next and see how an adiabatic wave tapering affects the particle. The coefficients $C_1$ and $C_2$ are presented in

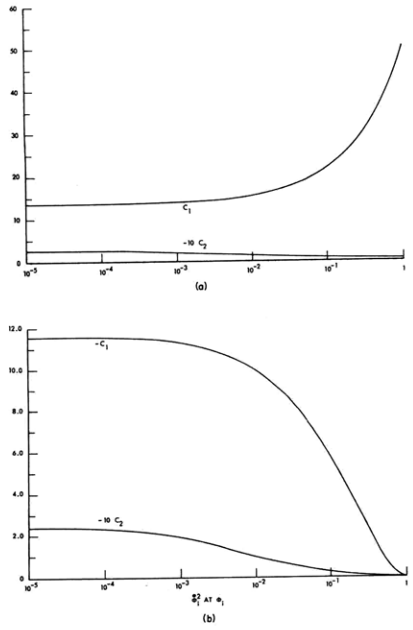


Fig. XVI-4. Plot of $C_1$ and $C_2$ vs $\dot{\phi}_i^2$, where $\Delta\dot{\phi}^2 = \dot{\phi}_f^2 - \dot{\phi}_i^2 = \alpha(C_1 + \lambda C_2)$ and $\gamma_i = 10^{-3}$.
(a) $\phi_i = 0$, $\phi_f = 2\pi$.
(b) $\phi_i = 2\pi$, $\phi_f = 0$.

Fig. XVI-4 as a function of $\dot{\phi}_i^2$ for $\gamma_i = 10^{-3}$ and for motion in the forward and reverse directions, respectively.

In the limit of small $\gamma_i$ and small $\dot{\phi}_i$, Eq. 6 simplifies to

$$\Delta\dot{\phi}^2 \equiv \dot{\phi}_f^2 - \dot{\phi}_i^2 = \pm 4\pi\alpha \sin(\dot{\phi}_i). \tag{7}$$

Several results follow. First, a particle with $\dot{\phi} > 0$ at a potential crest can never be trapped in a potential trough. Second, a particle with $\dot{\phi}_i < 0$ at a potential crest and $\dot{\phi}_i^2 < \dot{\phi}_{max}^2 = 4\pi a$ will be reflected by the next potential crest that it meets. Under the assumption of a uniform distribution of particles as a function of $\dot{\phi}_i^2$ over the limited range $0 < \dot{\phi}_i^2 < \dot{\phi}_{max}^2$, $(\dot{\phi}_i < 0)$, a certain fraction, $\eta_T$, will be trapped in the trough between those adjacent crests. Finally, for a uniform distribution in the range $0 < \dot{\phi}_i^2 < d^2$, $(\dot{\phi}_i < 0)$, with $d^2 \gg \dot{\phi}_{max}^2$, it follows from Eq. 7 that the same $\eta_T$ specifies the fraction trapped in any trough.

The quantity $\dot{\phi}_{max}$ $(\overline{\dot{\phi}_{max}} < 0)$ is defined by requiring a particle with $\dot{\phi}_i = \dot{\phi}_{max}$ at $\phi_i = 2\pi$ to have $\dot{\phi}_f = 0$ at $\phi_f = 0$. This trajectory is illustrated in the phase-plane diagram in Fig. XVI-5. Equation 6 is used to determine $\dot{\phi}_{max}^2$. It is convenient to take the limit $\dot{\phi}_{max}^2 \ll \gamma_i$, or equivalently, $a \ll \gamma_i$. Then

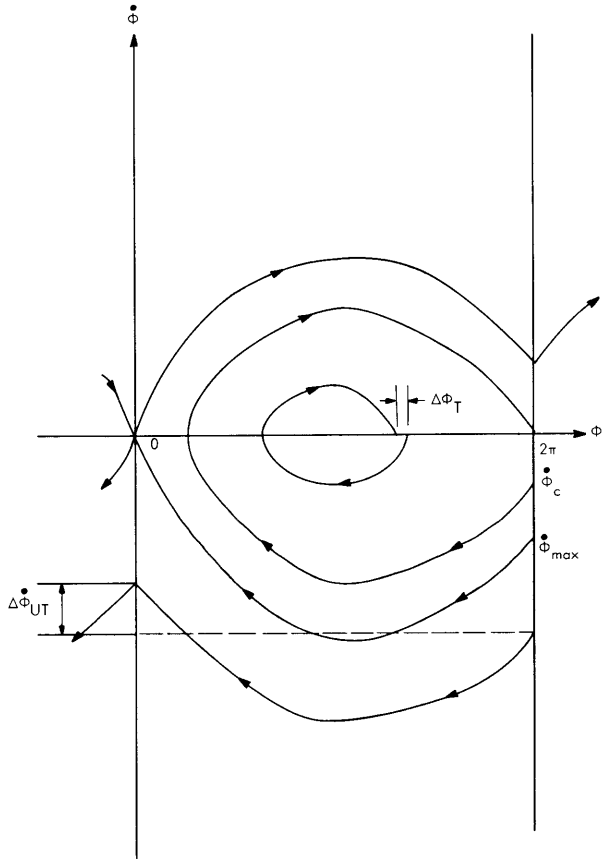


Fig. XVI-5. Phase-plane diagram illustrating trapped (T) and untrapped (UT) particle trajectories and the critical trajectories corresponding to $\dot{\phi}_i = \dot{\phi}_c$ and $\dot{\phi}_i = \dot{\phi}_{max}$.

$$\dot{\phi}^2_{max} = 4\alpha[\pi + 2\sqrt{\gamma_i}\,(\lambda-4) + \pi\gamma_i(2-\lambda)]. \tag{8}$$

To determine $\eta_T$, it is necessary to find the critical trajectory (see Fig. XVI-5) for the particle with $\dot{\phi}_i = \dot{\phi}_c < 0$ at $\phi_i = 2\pi$ and $\dot{\phi}_f = 0$ at $\phi_f = 2\pi$ after one oscillation. This particle is initially untrapped at one crest, it is reflected by the next crest, and reaches the original crest after "dissipating its excess energy." Figure XVI-5 is a sketch of the phase plane which illustrates the important trajectories. Adiabaticity guarantees that the Hamiltonian in terms of the variables $\phi, \dot{\phi}, \tau$ is a slowly varying function of time; therefore, the phase-plane trajectories are assumed not to intersect during the time interval displayed. It can be seen that $\dot{\phi}_c < \dot{\phi}_i < 0$ bounds the particles that will become trapped in that trough, while $\dot{\phi}_{max} < \dot{\phi}_i < \dot{\phi}_c$ bounds the untrapped particles. Therefore the trapped fraction is $\eta_T = \left(\dot{\phi}_c/\dot{\phi}_{max}\right)^2$, for particles uniformly distributed in $\dot{\phi}_i^2$. The quantity $\dot{\phi}_c^2$ can be determined from Eq. 6 when $\alpha \ll \gamma_i$. We find

$$\dot{\phi}_c^2 = 16\alpha\sqrt{\gamma_i}\,(\lambda-4). \tag{9}$$

Therefore,

$$\eta_T = \frac{4\sqrt{\gamma_i}\,(\lambda-4)}{\pi + 2\sqrt{\gamma_i}\,(\lambda-4) + \pi\gamma_i(2-\lambda)}. \tag{10}$$

(See Fig. XVI-6.) Equation 10 and Fig. XVI-6 are valid in the limit $\alpha/\gamma_i \to 0$. To investigate the required adiabaticity for these results, we made numerical computations of

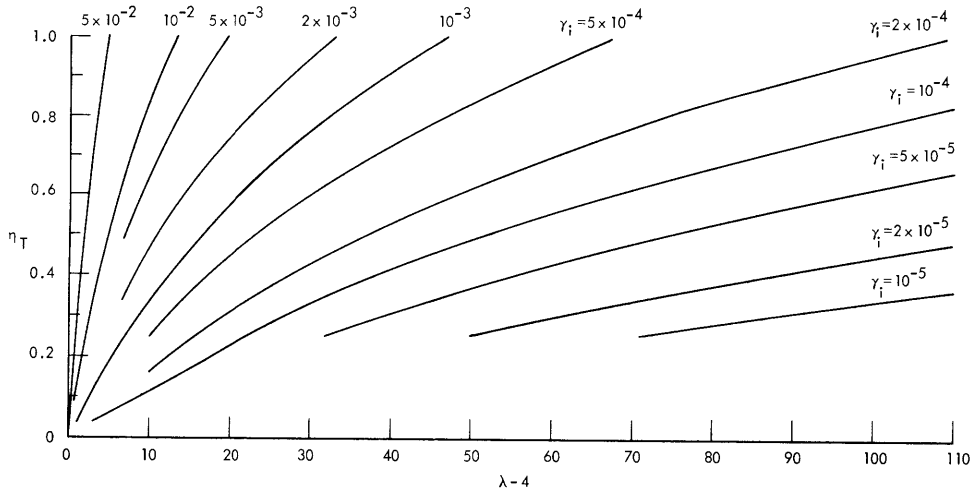


Fig. XVI-6. Relation between the fraction of particles trapped, $\eta_T$, and $\lambda - 4$ for several values of $\gamma_i$.

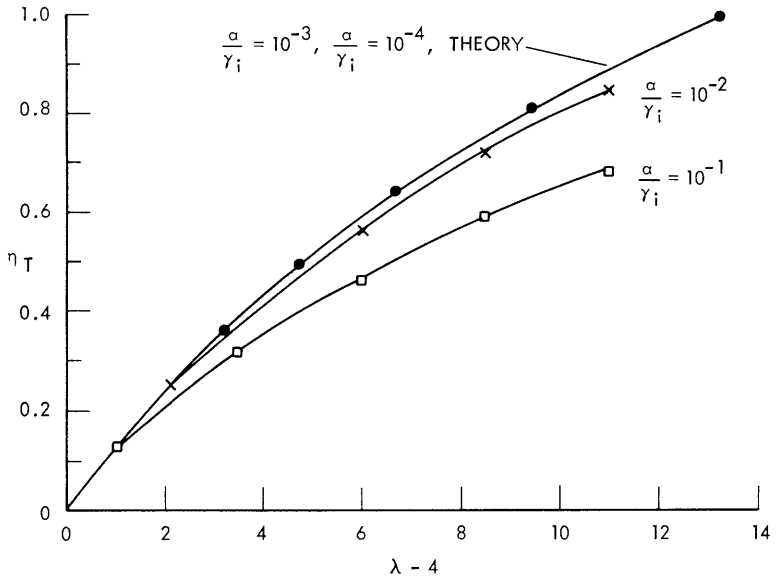


Fig. XVI-7. Comparison of the adiabatic theory determining $\eta_T$ vs $\lambda - 4$ (for $\gamma_i = 10^{-2}$), and the exact (numerically computed) results for several values of $\alpha$.

particle trajectories from the nonlinear equation of motion. The results shown in Fig. XVI-7 show how the numerical computations of $\eta_T$ approach the analytical values for several typical cases.

## Stability of Trapped Particles

We have seen that a nonzero percentage of initially untrapped particles becomes trapped in potential troughs of a decelerating wave if $\lambda > 4$. The next question is, Will these particles remain trapped? In other words, will the amplitude of phase oscillations be damped?

For small-amplitude phase oscillations, Eq. 1 can be linearized (with slowly varying coefficients) and solved by the WKB technique.[2] It is found that an equilibrium phase, $\phi_s$, exists only for $|\alpha| < \gamma$ and is defined by

$$\alpha + \gamma_i \sin \phi_s = 0. \tag{11}$$

These $\phi_s$ solutions can also be found from the extrema of the potential function[1]

$$V(\phi) = \gamma_i \cos \phi - \alpha\phi. \tag{12}$$

This potential function has trapped-particle troughs only for $|\alpha| < \gamma_i$. The amplitude of

phase oscillations for $|\alpha| \ll \gamma_i$ (stable $\phi_s \approx \pi$) is proportional to $v^{-1}\gamma^{-1/4}$. This result also applies to linear accelerators.[3] This WKB result also shows that the fractional change in the phase amplitude in one oscillation is

$$\frac{\Delta\phi}{|\phi-\phi_s|_{max}} = -\frac{\alpha(\lambda-4)\,\pi}{2\sqrt{\gamma_i}}. \tag{13}$$

Note that, if $\lambda > 4$, these small-amplitude oscillations are damped for $\alpha > 0$ (wave deceleration).

For large-amplitude phase oscillations, we can use Eq. 5 as previously to evaluate the "dissipation" over one oscillation, and thereby determine the change in the amplitude of oscillation. Figure XVI-8 shows the fractional change in phase amplitude

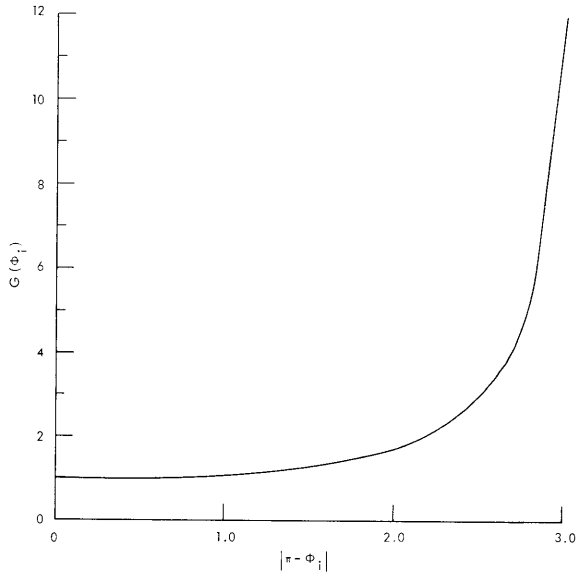


Fig. XVI-8. Illustration of $G(\phi_i)$ vs oscillation amplitude, where the fractional change in amplitude in one trapped particle oscillation is given by $\frac{\Delta\phi_T}{|\pi-\phi_i|} = \frac{\pi\alpha(\gamma-4)}{2\sqrt{\gamma_i}} G(\phi_i)$, and $|\pi-\phi_i|$ is the amplitude of phase oscillations.

normalized to the small-amplitude limit (13) as a function of peak phase amplitude. It is seen that $\lambda > 4$ is still the damping condition, with large-amplitude oscillations damping more than small-amplitude oscillations.

Discussion and Conclusions

To summarize, $\lambda = 4$ is the minimum condition for keeping all trapped particles trapped. With $\lambda > 4$, the phase oscillations of the trapped particles are damped and a fraction of untrapped particles becomes trapped as they approach synchronism with the decelerating wave.

By using a perturbation approach, it can be shown that the change in energy of untrapped particles compared with trapped ones is of order $\gamma$ (which should be kept much less than one); particles moving faster than the wave lose energy, while those moving slower gain energy. If $\eta_T$ is nearly unity, the energy change of these untrapped particles can be ignored in evaluating the overall efficiency.

With this information, it is now possible to determine the required phase speed and wave amplitude tapering for the full length of the converter in order to achieve high recovery efficiencies. First, assume that the ion distribution function is uniformly distributed in energy with an energy spread of $\Delta E$, centered at E. If we ask for a constant trapping efficiency throughout the device, then by using Eq. 10, we find the wave phase speed v(z) vs normalized wave amplitude $\gamma(z)$ shown in Fig. XVI-9. The final phase velocity should be as low as possible for efficient energy recovery, but as $\gamma$ approaches 0.1, the oscillation energy of trapped particles becomes significant, thereby reducing the recovery efficiency. For this reason, the straightfoward

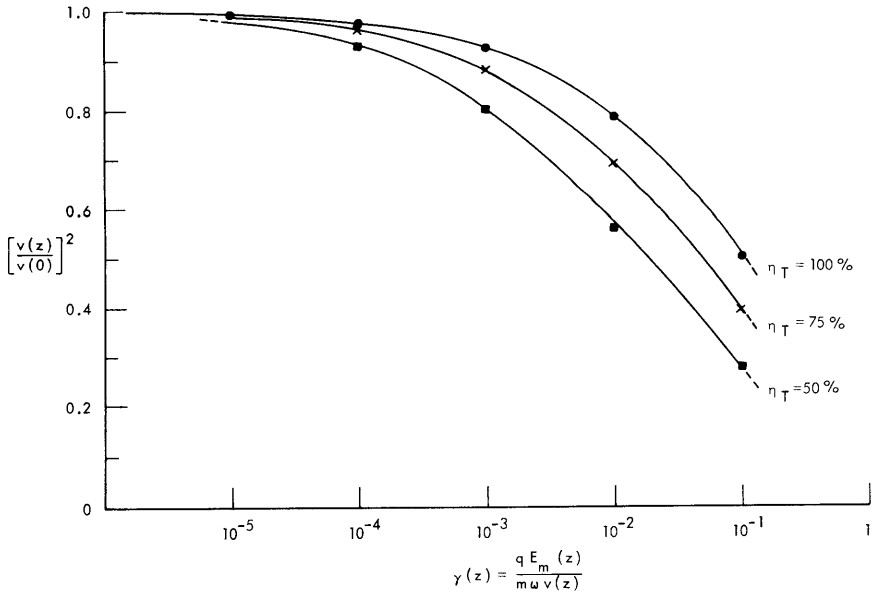


Fig. XVI-9. Required wave taperings, phase velocity vs amplitude, for several values of constant trapping efficiency.

application of decelerating wave techniques does not seem to be capable of attaining high recovery efficiencies from very broad ion energy distributions.

High efficiencies can be realized with relatively narrow energy spreads, however. To maximize the recovery efficiency of ion streams with a narrow energy spread, the $\eta_T = 100\%$ curve in Fig. XVI-9 is followed until all of the particles are trapped; then the wave amplitude is varied in a manner to contain all trapped particles as the wave continues to slow down (that is, the $\lambda = 4$ taper is followed) until $\gamma$ reaches 0.1. The energy recovery efficiency as a function of energy spread with this taper is estimated to be limited to the upper bound given by

$$\eta_R = 1 - 1.37\,(\Delta E/E). \tag{14}$$

Energy spreads less than 10% could therefore lead in principle to recovery efficiencies approaching 90%.

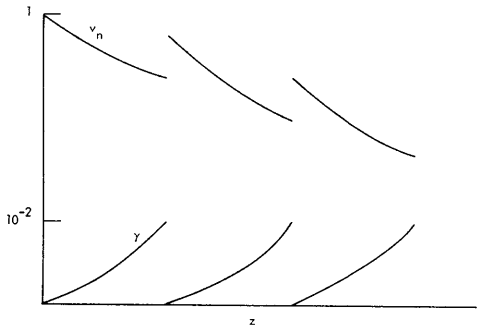


Fig. XVI-10. Cyclic tapering scheme for $v_n(z)$ and $\gamma(z)$.

To handle large ion energy spreads efficiently, the "cyclic tapering" illustrated in Fig. XVI-10 might be used. For example, in each segment the constant trapping efficiency taper is used until $\gamma \approx 0.01$. Then power is removed from the line ($\gamma$ is reduced to a very small value), while v is increased to compensate for the oscillation energy in the well. Detailed considerations indicate that the maximum recovery efficiency for this method would be approximately 75%.

M. I. Mirkin, R. J. Briggs

## References

1. M. I. Mirkin and R. J. Briggs, Quarterly Progress Report No. 101, Research Laboratory of Electronics, M.I.T., April 15, 1971, pp. 137-142.

2. G. F. Carrier, M. Krook, and C. E. Pearson, Functions of a Complex Variable (McGraw-Hill Book Co., New York, 1966), pp. 291-294.

3. A. D. Vlasov, Theory of Linear Accelerators (translated from Russian by Z. Lerman), Program for Scientific Translations, Jerusalem, Israel, 1968, p. 29.

# XVI. APPLIED PLASMA RESEARCH*

## B. Plasma Physics and Engineering

### Academic Research Staff

Prof. R. A. Blanken
Prof. T. H. Dupree
Prof. E. P. Gyftopoulos
Prof. L. M. Lidsky

### Graduate Students

J. R. Aument
G. W. Braun
A. R. Forbes
J. C. Hsia
B. H. Hui
G. D. Pine
C. A. Primmerman

### RESEARCH OBJECTIVES

1. Nonlinear and Turbulence Theory of Plasmas

Plasma processes that depend upon particle discreteness can be greatly enhanced by the tendency of turbulent plasma to develop small-scale phase space granulations, or clumps. Such granulations can, in some circumstances, behave as single large particles, or macroparticles. We propose to derive and solve the equations for clump formation and evolution. We hope to apply this theory to a variety of physical problems. We shall continue our study of nonlinear dispersion relations for both high- and low-frequency instabilities; particularly, we intend to use the dispersion relation to predict the saturation levels and other turbulence properties measured in several recent experiments.

T. H. Dupree

2. Turbulence and Diffusion in a Highly Ionized Plasma Column

Although it is generally agreed that fluctuating electric fields are the cause of experimentally observed enhanced plasma transport, the expected quantitative relations between the magnitude and frequency of the fluctuations and the speed and direction of transport are not often satisfied. We have developed a new technique from the direct measurement of diffusion flux and are using it to investigate plasma flows in a radio-frequency produced collisionless plasma column. We have discovered large-scale rotating vortices that appear to be the nonlinear limit of the Kelvin-Helmholtz shear instability. We shall try to understand their role in transport and compare the non-linear saturated state to theoretical predictions. Various externally imposed instability damping techniques will be tested.

L. M. Lidsky

3. Study of Anomalous Resistivity

The highly ionized plasma column will be used to measure plasma resistivity in the regime in which the electron drift velocity is comparable to the ion acoustic velocity. We hope to eliminate the problem of unknown sheath voltage drops by using large-area emitting electrodes as current source and sink.

C. A. Primmerman, L. M. Lidsky

---

*This work is supported by the National Science Foundation (Grant GK-28282X).

4. Far Infrared Plasma Diagnostics

We plan to construct several dual-purpose lasers that will operate on either HCN or $H_2O$. Suitable optics will be developed and the lasers used for diagnostics in several plasma experiments. The 337-μm HCN line is particularly suitable for use in our experimental investigations of velocity space instabilities.

J. C. Hsia, R. A. Blanken

5. High-Power Laser Development and Applications

The high-power TEA laser will be investigated in an effort to develop a light source suitable for plasma diagnostics in the coherent regime. Such a laser might, for example, be used in Alcator to measure the radial distribution of ohmic heating current. The transverse-flow cw laser will be further investigated in our continuing effort to develop a low-cost stabilized discharge laser in the 500-1000 W range. This is suitable for laboratory studies (electrode-heating thermionic diodes and plasma sources, for example) and various industrial uses.

L. M. Lidsky

# XVI. APPLIED PLASMA RESEARCH*

## C. Plasma Effects in Solids


Academic Research Staff

Prof. A. Bers

Graduate Students

J. F. Cafarella


### RESEARCH OBJECTIVES AND SUMMARY OF RESEARCH

During the past year we have continued our studies on the interaction between acoustic surface waves on piezoelectrics with electron-plasma surface waves on semiconductors. The latter are particularly weakly damped in crossed electric and magnetic fields, and can either passively couple to, or amplify, the acoustic surface wave. Experiments have been carried out which give a confirmation of these interactions in a magnetic field. A complete theoretical analysis of such interactions has also been developed.[1]

For the next year, we plan to study the direct electrical excitation of surface waves on a semiconductor. In addition, we plan to use the surface acoustoelectric interaction for determining the transport characteristics of electrons at the surface of semiconductors.

A. Bers

References


1. A. Bers, "Interactions between Acoustic Surface Waves and Electrons in Solids," Invited Proceedings of the 1970 IEEE Ultrasonics Symposium, San Francisco, California, October 21-23, 1970, IEEE Publication No. 70 C 69 SU, New York, 1971, pp. 138-172.


### 1. SURFACE ACOUSTOELECTRIC CURRENT AND SURFACE MOBILITY OF ELECTRONS

#### Introduction

Acoustic surface waves on piezoelectrics can be amplified by drifting electrons on an adjacent semiconductor. A practical amplifier of this type, at high frequencies ($10^8$-$10^9$ Hz), has been developed recently by accumulating the electrons at the semiconductor surface adjacent to the piezoelectric.[1] The density of electrons in the accumulation layer can be easily controlled and measured by well-known means. The mobility of these electrons is much less understood, and is difficult to measure because of surface states or traps. We propose to measure the surface mobility of these


*This work was supported by the National Science Foundation (Grant GK-28282X), and in part by M. I. T. Lincoln Laboratory Purchase Order No. CC-544.

electrons through a passive surface acoustoelectric interaction, the surface acoustoelectric current. This direct current flows in the semiconductor whenever an acoustic surface wave propagates on the adjacent piezoelectric. There are several advantages in this way of determining the mobility: (a) the measurements can be made at sufficiently high frequencies where surface states can be ignored; (b) the measurements can be made with no applied electric field on the semiconductor, thereby avoiding hot-electron effects on the mobility; (c) the mobility variation with band bending can also be determined. We shall describe the effects of trapping in the surface acoustoelectric interaction, and in the acoustoelectric current. We shall then show that for high frequencies the measurement of the acoustoelectric current and acoustic-wave damping gives the surface mobility.

## Effect of Traps on the Accumulation Layer Interaction with Acoustic Waves

The dispersion relation for the accumulation layer surface-wave amplifier is known.[1] The accumulation layer was modeled as a sheet conductance over a dielectric substrate, and the semiconductor properties were expressed in terms of an effective sheet conductivity, $\sigma_s(\omega, k)$. This conductivity will now be modified to reflect the presence of traps.

The small-signal, ac properties of the semiconductor are described by the continuity and (linearized) current equations

$$kK_1 = \omega n_{s1} \tag{1}$$

$$K_1 = q\mu n_{so} E_1 + q\mu n'_{s1} E_o - qDkn'_{s1}, \tag{2}$$

where $K_1$ is the small-signal sheet current density; $n_{s1}, n'_{s1}$, the small-signal bunched electron sheet density; $q, \mu$, the electron charge magnitude and surface mobility; D, the electron diffusion coefficient; and $\omega, k$, the radian frequency and wave number. Two types of bunched densities $n_{s1}$ and $n'_{s1}$ appear because not all bunched electrons are free to move, some being held in traps. In the continuity equation we must consider the total bunched sheet density, $n_{s1}$, while in the current equation we must use only $n'_{s1}$, the bunched charge which is free to move. Thus we define the trapping factor

$$f \equiv \frac{n'_{s1}}{n_{s1}} = \frac{n'_{s1}}{n'_{s1} + n_{t1}}, \tag{3}$$

where $n_t = n_{s1} - n'_{s1}$ = trapped bunched density. The sheet conductivity function becomes

$$\sigma_s(\omega,k) = \frac{\omega\sigma_{so}}{\omega - kfv_o - jDfk^2}, \tag{4}$$

where $\mu_{so} = q\mu n s_o$, and $v_o = \mu E_o$.

This enables modification of previous results,[1] which depend upon $\sigma_s(\omega, k)$, to account for traps. In general, f is complex and depends upon the radian frequency $\omega$.

Surface Acoustoelectric Current

In the linear analysis, which gave $\sigma_s(\omega,k)$, the nonlinear current $qn'_{s1}E_1$ was neglected as second order. The time average of this nonlinear current is a dc (acoustoelectric) current that accompanies the interaction. From the complex amplitudes of the linear analysis, this sheet current is

$$K_{AE} = \frac{1}{2} q\mu \text{ Re}\{n'_{s1}E_1^*\} = \frac{1}{2}\mu q \text{ Re}\{fn_{s1}E_1^*\}. \tag{5}$$

By using charge conservation and the effective conductivity (Eq. 4),

$$K_{AE} = \frac{q\mu}{2v_s} |E_1|^2 \text{ Re}\{f\sigma_s(\omega, k)\}, \tag{6}$$

where $v_s$ is the acoustic wave velocity.

The electric field may be related to the acoustic power flow by using a complex power theorem[2] and an effective dielectric function[3] for the acoustic medium,

$$|E_1|^2 = \frac{4k_i P_A}{\text{Re}\{\sigma_s(\omega, k)\}}, \tag{7}$$

where $P_A$ is the acoustic power density per unit width, and $k_i$ is the imaginary part of the propagation constant. Using Eq. 7, $|\text{Re}\, f| \gtrsim |\text{Im}\, f|$, and $|\text{Re}\,\sigma_s(\omega, k)| \gg |\text{Im}\,\sigma_s(\omega, k)|$, for usual semiconductor parameters, we have

$$K_{AE} = \frac{\mu}{v_s} 2k_i P_A (\text{Re}\, f). \tag{8}$$

This effective source current within the semiconductor may be related to the short-circuit current measured at the terminals.[4]

$$I_{AE} = \frac{\mu}{v_s} \frac{P_D}{L} \text{Re}\, f, \tag{9}$$

where L is the interaction length, and $P_D$ is the acoustic power dissipated in L. Since $P_D$, L and $v_s$ are otherwise measurable, the acoustoelectric current measurement gives the product $\mu(Ref)$.

Frequency Dependence of Trapping Factor

We treat the accumulation layer as a sheet of electrons with density $n_s$ given by

$$n_s = \int_0^{\infty} n(x)\, dx, \tag{10}$$

where n(x) is bulk electron density as a function of x, the depth into the semiconductor. We also treat the traps as a sheet of surface states with energies distributed within the energy gap, $N_{ss}(E)$. The following trapping dynamics may be formulated for traps at energy E:

$$\frac{d}{dt}\left(\frac{dn_t}{dE}\right) = c(E)\, n_s N_{ss}(E)(1-F(E)) - e(E)\, N_{ss}(E)\, F(E), \tag{11}$$

where $n_t$ is the trapped electron density; F(E), the Fermi distribution function; c(E), the capture probability for the empty trap; $N_{ss}(E)$, the density of traps; (1-F(E)), the fraction of empty traps; e(E), the expulsion probability of the full trap.

At equilibrium the net capture rate d/dt ($dn_t/dE$) is zero, hence

$$\frac{c(E)}{e(E)} = \frac{n_{so}(1-F_o(E))}{F_o(E)}. \tag{12}$$

If we linearize for small signals, assume exp(jωt) dependence, and recognize that $N_{ss}(E)\, F_1(E) = dn_{t1}/dE$, we have

$$\frac{dn_{t1}}{dE} = \frac{n_{s1}}{n_{so}}\left[\frac{N_{ss}(E)\, f_o(E)(1-F_o(E))}{1 + j\dfrac{\omega F_o(E)}{n_{so}c(E)}}\right]. \tag{13}$$

The trapping factor is given by Eq. 3, which may be evaluated from

$$\frac{1}{f} - 1 = \frac{n_{t1}}{n_{s1}} = \frac{1}{n_{so}} \int_{E_v}^{E_c} \frac{N_{ss}(E)\, F_o(E)(1-F_o(E))\, dE}{1 + j\dfrac{\omega F_o(E)}{n_{so}c(E)}}. \tag{14}$$

The product $F_o(E)(1-F_o(E))$ is sharply peaked about the Fermi energy $E_F$. If we assume that $N_{ss}(E)$ varies slowly compared with $F_o(E)(1-F_o(E))$ and that c(E) is constant, we may evaluate the integral.[5] The limits of integration may be extended to $\pm\infty$, which makes little difference because of the dominance of $F_o(E)(1-F_o(E))$.

At low frequencies the traps remain in equilibrium with the electrons, and the trapping factor approaches a constant $f_o$.

$$\lim_{\omega\to 0} \frac{1}{f} - 1 = \frac{1}{f_o} - 1 = \frac{N_{ss}(E_F)}{n_{so}} \int_{-\infty}^{\infty} F_o(E)(1-F_o(E))\, dE = \frac{\kappa T N_{ss}(E_F)}{n_{so}}. \tag{15}$$

At any frequency the expression for $\frac{1}{f} - 1$ becomes

$$\frac{1}{f} - 1 = \left(\frac{1}{f_o} - 1\right) G(\omega), \tag{16}$$

where

$$G(\omega) = \frac{1}{\kappa T} \int_{-\infty}^{\infty} \frac{F_o(E)(1-F_o(E))\, dE}{1 + j \dfrac{\omega F_o(E)}{n_{so} c}}. \tag{17}$$

Note that $\lim_{\omega\to 0} G(\omega) = 1$, and $\lim_{\omega\to\infty} G(\omega) = 0$.

We use two methods to evaluate the integral. In the first method we approximate $F_o(E)(1-F_o(E))$ by $\kappa T \delta(E-E_F)$.

$$G_1(\omega) = \int_{-\infty}^{\infty} \frac{\delta(E-E_F)\, dE}{1 + j \dfrac{\omega F_o(E)}{n_{so} c}} = \frac{1}{1 + j \dfrac{\omega\tau}{2}}, \tag{18}$$

where $\tau \equiv \frac{1}{n_{so} c}$. In the second method[5] it is recognized that $\frac{1}{\kappa T} F_o(E)(1-F_o(E)) = -\frac{dF_o(E)}{dE}$. The limits of integration change from $(-\infty, +\infty)$ to (1, 0).

$$G_2(\omega) = \int_0^1 \frac{dF_o}{1 + j \dfrac{\omega F_o}{n_{so} c}} = \frac{\ln(1+j\omega\tau)}{j\omega\tau}. \tag{19}$$

$G_1(\omega)$ and $G_2(\omega)$ are compared in Fig. XVI-11. While $G_2(\omega)$ is an exact solution, $G_1(\omega)$ is of sufficient accuracy and simplicity to warrant its use.

We see here a very important property of the trapping factor. No matter what the detailed frequency dependence, the trapping factor approaches unity for $\omega\tau \gg 1$. The reason for this is that the variations in free-electron density occur so rapidly that the traps retain a steady density of trapped electrons rather than readjust to the free-electron fluctuations. Under these conditions the acoustoelectric current no longer depends on trapping, and we have a direct measurement of $\mu$ (see Eq. 9) which we can compare with other measurements.[6]

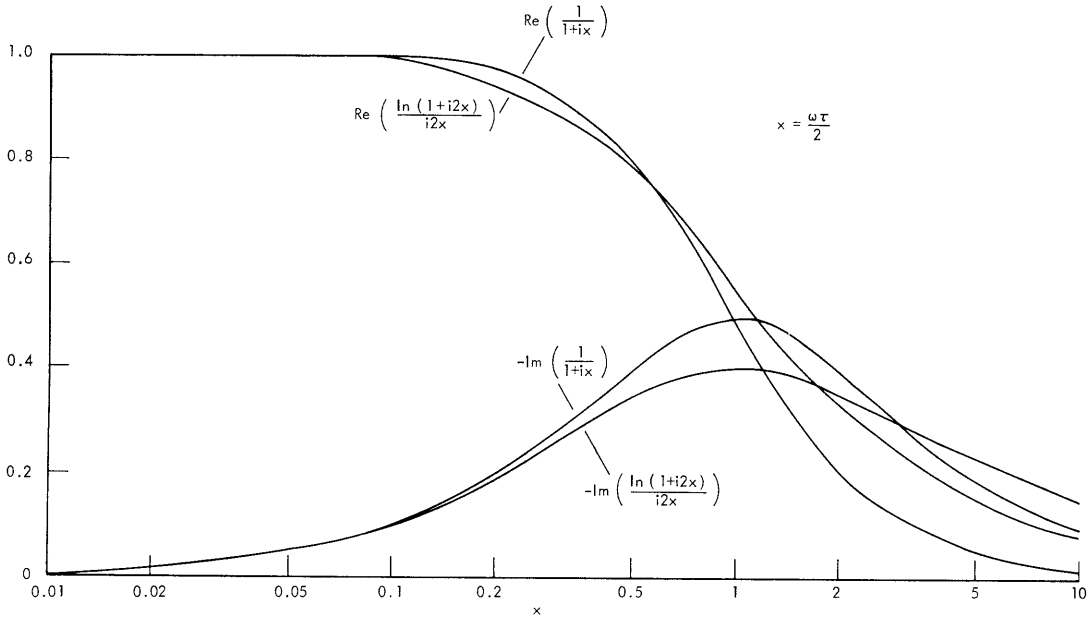


Fig. XVI-11. Real and imaginary parts of $G_1(\omega)$ and $G_2(\omega)$.

## Conclusion

We have at our disposal a technique, the use of the acoustoelectric current, which allows determination of the product $\mu(\mathrm{Re}\, f)$. Our primary interest is in measuring the electron surface mobility. Our analysis has shown that the trapping factor approaches unity at high frequencies, $\omega\tau \gg 1$. Hence measuring the acoustoelectric current in this range of frequencies gives $\mu$ directly. The relaxation time for traps, $\tau$, is given by $\tau = 1/n_{so}c$, where $n_{so}$ and $c$ are sheet quantities. For a rough estimate of the range of $\tau$ we may use bulk parameters.[5] For the bulk $\tau = \frac{1}{\sigma_c v_t n_o}$ ($\sigma_c$ = capture cross section $\sim 10^{-15}$ cm$^2$; $v_t$ is the thermal velocity $\sim 10^7$ cm/s; $n_o$ is the bulk electron density $10^{11} < n_o < 10^{19}$). The range of $\tau$ is $10^{-11}$ s $< \tau < 10^{-3}$ s. The range of frequencies over which surface acoustic interactions are readily made is $10^8$-$10^9$ Hz. Since we can control the density in the accumulation layer with a transverse electric field, we may choose a range of densities for which we then satisfy $\omega\tau \gg 1$. This work is being carried out in collaboration with the Microsound Group at Lincoln Laboratory, M. I. T.

J. F. Cafarrella, A. Bers

## References

1. B. E. Burke, A. Bers, H. I. Smith, R. A. Cohen, and R. W. Mountain, Proc. IEEE 58, 10 (1970).

2. W. P. Allis, S. J. Buchsbaum, and A. Bers, "Waves in Anisotropic Plasmas (The M. I. T. Press, Cambridge, Mass., 1963).

3. A. Bers, "Interactions between Acoustic Surface Waves and Electrons in Solids," Invited Proceedings of the 1970 IEEE Ultrasonics Symposium, San Francisco, California, October 21-23, 1970, IEEE Publication No. 70 C 69 SU, New York, 1971, pp. 138-172.

4. K. A. Ingebrightsen, J. Appl. Phys. 41, 2 (1970).

5. E. H. Nicollian and A. Goetsberger, Bell Syst. Tech. J. 46, 6 (1967).

6. O. Leistiko, Jr., A. S. Grove and C. T. Sah, "Electron and Hole Mobilities in Inversion Layers on Thermally Oxidized Silicon Surfaces," IEEE Trans., Vol. ED-12, No. 5, pp. 248-254, May 1965.